INTERNATIONAL JOURNAL OF FLUID POWER, 2016
VOL. 17, NO. 3, 187–201
http://dx.doi.org/10.1080/14399776.2016.1202081

Taylor & Francis
Taylor & Francis Group

Fuel optimal controller for hydrostatic drives and real-world experiments on a wheel loader

Joni Backas, Reza Ghabcheloo, Seppo Tikkanen and Kalevi Huhtala

Department of Intelligent Hydraulics and Automation, Tampere University of Technology, Tampere, Finland

ABSTRACT

In this study, we design a fuel optimal controller for hydrostatic drive transmissions (HSD) that significantly improves their fuel economy. Contrary to great proportion of the literature, efficacy of the controller is demonstrated by real machine implementation equipped with online fuel consumption measurement system. The main control objective of the devised controller is to minimise consumed fuel per travelled distance. Control commands are determined utilizing steady-state equations of the system, which facilitates real-time implementation. Dynamic situations are addressed with auxiliary functions running at higher frequency than the fuel economy part of the controller. The machine is a 5-ton wheel loader with pure HSD and no energy storage devices installed. In addition, all the components are commercially available. Thus, structure of the HSD and presented improvements in fuel economy are comparable to commercial machines and retrofitting existing drive-by-wire machinery with proposed controller will require little cost. The optimal controller is compared to a rule-based alternative that is based on a control method utilized in commercial wheel loaders. In autonomously driven drive cycles, measured total fuel consumption reduced up to 16.6% with the devised controller. In addition, the functionality of the controller is proven in extreme hill climbing tests.

ARTICLE HISTORY
Received 25 January 2016
Accepted 13 June 2016

KEYWORDS
Fuel economy; power management; energy efficiency; power transmission; non-road mobile machinery

1. Introduction

Invariably decreasing oil resources and the growing number of machines operated by fossil fuels increase the demand for energy efficient solutions in the different fields of industry and transportation. Investigations in fuel economical technologies for passenger cars have been a very active field of research already for a long time. In 1997, Toyota Prius, the first mass produced hybrid vehicle, was introduced. However, the same statement cannot be made for machines utilized in construction industry, even though their estimated annual fuel consumption in European Union was 18.6 million tons (Arcadis 2010) and their emissions produce a significant burden on the environment. These machines generally use hydraulic power transmissions due to high power density requirement. However, due to utilized system configurations and control methods in commercial machines, hydraulic systems exhibit higher energy losses compared to their electric alternatives.

In recent years, some hydraulic hybrid concept machines have been presented at exhibitions by e.g. John Deere (The Lubrizol Corporation 2013) and Kawasaki (KCMA Corporation 2011), but due to their cost, their widespread use is limited. However, improving the energy efficiency of non-road mobile machines (NRMM) does not necessarily require additional components or systems such as energy storages. We show in this paper that considerable fuel savings can be achieved by improved control strategy of electronically controlled hydraulic actuators. Thus, mechanical complexity, initial investment and maintenance costs are kept low. Still, the proportion of these drive-by-wire machines in non-road applications is quite low. This is mostly due to the fact that the field is very cost-conscious and the payback time of new systems should be short. We believe the application of fuel optimal strategies presented in this paper will reduce the consumption to a level that the increased price of drive-by-wire machines is justified.

The key factor for higher fuel economy is adjusting the operation points of the control components of the machine according to load and velocity. But because loading conditions constantly change, it is not possible for the driver to operate the machine optimally without the assistance of computer. This requires a drive-by-wire machine and intelligent control strategy.

In automotive industry, electronically controlled actuators have been utilized widely for a long time. Different power management strategies are still actively researched both by the academia and industry. Continuously variable transmissions offer significant improvements of

CONTACT Joni Backas joni.backas@tut.fi

fuel economy for non-hybrid passenger cars with the cost of increased control complexity (Pfiffner *et al.* 2003, Srivastava and Haque 2009). During the recent years, especially control of hybrid electric vehicles (HEV) and hydraulic hybrid vehicles (HHV) have been investigated extensively. Power management solutions of HEVs include a number of different methods reviewed e.g. in Sciarretta and Guzzella (2007). Even though HHVs are not as widely researched as HEVs, similar approaches are used in their power management as well. The most utilized strategies, suitable also for real-time implementation, are rule-based (Filipi *et al.* 2004, Kum *et al.* 2011, Hippalgaonkar and Ivantysynova 2012) equivalent consumption minimisation strategy (Paganelli *et al.* 2001, Sciarretta *et al.* 2004, Serrao *et al.* 2011), model predictive control (MPC) (Feng *et al.* 2011, Kermani *et al.* 2011, Deppen *et al.* 2012) and stochastic dynamic programming (SDP) (Meyer *et al.* 2010, Opila *et al.* 2013).

Usually NRMMs have at least partially hydraulic drive transmissions, and there are no commercial hybrid drive transmissions available for them. Nevertheless, there is a growing interest towards improving the inherently low efficiency of fluid power systems and several academic departments are focusing on this kind of machines. Rule-based, MPC and SDP strategies were compared in laboratory experiments for HHV transmission by Deppen *et al.* (2015). They emulated diesel engine with an electric motor, and load with a hydraulic motor both controlled with appropriate simulation models. The improvements of fuel economy were determined with brake specific fuel consumption (BSFC) maps of the modelled engine. Their main conclusion was that no control method can be considered superior in all applications and choosing the most appropriate one has to be made based on assumed system and drive cycle. Kumar and Ivantysynova (2011) used similar test set-up, but their transmission had also mechanical path between the load and the emulated gasoline engine of Toyota Prius. The system was controlled with instantaneous optimisation based algorithm. Also the control of non-hybrid drive transmission has been investigated by Jähne *et al.* (2008). They compared demand-adapting engine speed with two other control concepts in their simulation study. In the research of Ahopelto *et al.* (2013), similar approach was utilized in the field tests of a wheel loader. In addition, the energy efficiency improvements of other subsystems of NRMM have been investigated, e.g. steering by Daher and Ivantysynova (2014), implement hydraulics by Huova *et al.* (2010) and the swing motion of excavator by Catepillar Inc. (2013).

Despite the numerous published results about novel controllers for HEVs, HHVs and NRMMs, there seems to be a significant gap between simulation studies and reported hardware tests. Even more noteworthy is the lack of research in which the success is evaluated with real fuel consumption instead of e.g. modelled steady–steady efficiencies. However, some exceptions with measured improvement can be found. Wang *et al.* measured fuel consumption of HEV powertrain in laboratory test bench with similar equipment that is used in this paper (Wang *et al.* 2013). Paganelli *et al.* determined consumed fuel volume and corrected the number with the difference of battery state of charge (Paganelli *et al.* 2001). Williamson weighted external fuel tank (Williamson 2010) and Ahopelto *et al.* presented the fuel consumption data provided by the electronic control unit of the engine (Ahopelto *et al.* 2013).

In this paper, we utilize optimal control methods to define control commands for the components of hydrostatic drive transmission (HSD), namely diesel engine, variable displacement hydraulic pump and hydraulic motors. This optimal control combination is solved on given velocity reference, demanded load and efficiency curves. The algorithm does not utilize information about the complete cycle. Therefore, the results differ from global optima. It is important to note that in our test setup all the components of HSD are commercially available and there are no energy storage components installed. Moreover, the developed algorithm can be executed in commercial programmable logic controllers (PLC) due to its relative simplicity and adjustability. This makes our results applicable to current machines equipped with CAN bus controlled components without any changes in their mechanical design. In this study, we use a 5-ton wheel loader as research platform. The consumed fuel is measured on-line and the collected data proves that drive-by-wire operation has even more to offer than just reduced number of hoses and more user-friendly interfaces.

The empirical tests were conducted in the test area of the Department of Intelligent Hydraulics and Automation (IHA) of Tampere University of Technology (TUT). The area includes both asphalt and gravel surfaces, and slopes up to 20 degrees. Unlike the majority of energy management studies, we present online measured fuel consumption data to show the efficacy of our control strategy. The repeatability of the experiments is guaranteed by generating the references with computers instead of human operators.

For comparison purposes, a rule-based controller was devised. This controller is very similar to the way some machine manufacturers control their HSD systems. In this rule-based control, the engine command is proportional to velocity reference, and hydraulic displacement ratio is varied depending on the measured engine speed. Similar baseline controllers are also utilized in Jähne *et al.* (2008).

We will show that fuel economy can be improved up to 16.6%, when the optimal controller is compared to the rule-based controller. Moreover, the controllability and performance of the system is also preserved. The field tests agree with the simulation results the authors

reported in Backas *et al.* (2014). Based on the test results, we can confidently state that the main factor for reduced fuel consumption is the active control of the rotational speed of diesel engine. This may cause the loss of controllability, which is addressed in this paper.

Next section presents the research platform and related equations. This is followed by sections covering the optimal controller and the control architecture of the machine. The last part of the paper presents the results of empirical tests with the two controllers.

2. System description

In this section, we introduce the research platform machine, namely its HSD and the control systems. For more detailed description of the systems of the machine, an interested reader is referred to Backas *et al.* (2011). Moreover, we describe and derive the steady-state equations of translational motion of the machine to be used by the optimal controller.

2.1. Research platform machine

The research platform, called IHA-machine, is engineered at the Department of IHA in TUT. The machine is presented in Figure 1.

Figure 1. Research platform.

2.1.1. Hydraulic system

The HSD of the machine is a closed hydraulic circuit. This means that the fluid utilized in the transfer of power is fed back to the pump from the motors, instead of being circulated through a tank. A simplified diagram of HSD is presented in Figure 2.

The prime mover, a 100-kW diesel engine, provides power to a hydraulic pump connected directly to the engine. The pump is variable displacement type, i.e. its output flow (see Q_p of Figure 2) can be controlled both by its swash plate angle (displacement) and by the speed of the engine shaft n_e. Moreover, the pump can provide flow in both directions allowing forward and reverse motion. The produced volumetric flow is directed to 4 hydraulic motors connected to each wheel of the machine. The displacement ratios of these hub motors (ε_m) can be changed between two discrete settings, full and 50% of

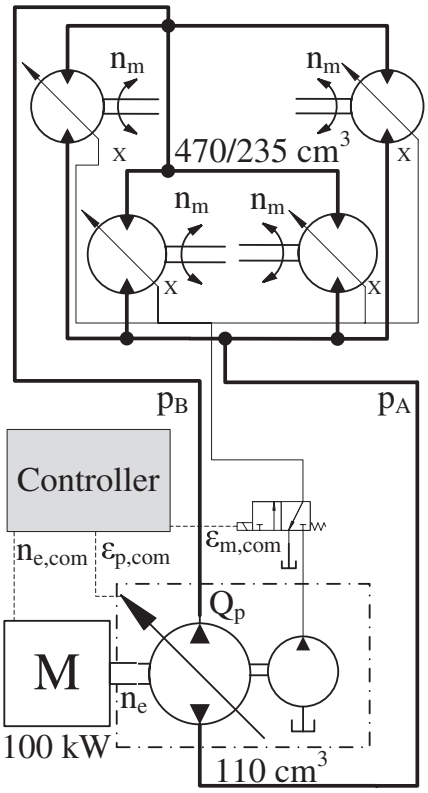

Figure 2. Hydrostatic drive transmission of the research platform machine.

the maximum. This is done by 'short-circuiting' feed and return ports of the motors together during half of their piston strokes. With reduced displacement, the velocity of the machine can be approximately doubled only by changing the control command of the motors $\varepsilon_{m,\mathrm{com}}$. However, this will reduce the maximum available output torque the same proportion. The steady-state equations of the system are presented in Section 2.2.2. The maximum displacements of the HSD pump (V_p) and motors (V_m) are 110 and 470 cm^3, respectively. Variables p_A and p_B are the pressures of volumes A and B, respectively.

2.1.2. Control electronics

The devised controller is realised in Matlab Simulink environment and implemented in the research platform with an embedded PC board running xPC target. The low level actuator controllers of the HSD pump and diesel engine are designed by their manufacturer. Both the command of the pump ($\varepsilon_{p,\mathrm{com}}$) and the engine ($n_{e,\mathrm{com}}$) are transmitted via CAN bus to the on-board-electronics of these components that implement the closed loop control of the displacement ratio of HSD pump (ε_p) and the rotational speed of engine. The command of HSD motors is amplified with a commercial control unit which operates the control valve of Figure 2.

2.1.3. On-line fuel consumption measurement

In contrast to majority of fuel economy researches, we present measured real-time fuel consumption data. The utilized hardware is a KMA Mobile by AVL. This device

enables measuring fuel flows from 0.16 to 75 l/h also in transient situations, because its rise time (10–90%) is smaller than 125 ms. The flow metre is based on the Pierburg measuring principle, and its measurement uncertainty is 0.1% of reading. (AVL 2009) The acquired data is sent to CAN bus with 20-Hz frequency. Use of the unit increases the accuracy and reliability of data for short tests.

2.2. Problem formulation

In this section, we derive the necessary equations for the fuel optimal control of HSD. First, we describe the inputs and outputs of the system. Then utilized cost function is introduced, from which we proceed to the equations that can be evaluated with the measured values of the states of the system.

2.2.1. Control objectives

Our control objective in words can be expressed as follows. Given a geometrical path to follow and a reference speed profile,

(1) Minimise the amount of fuel consumed.
(2) Minimise the velocity error for given reference trajectory.

The optimal controller attempts to meet these objectives by determining the control combination $\boldsymbol{u}$ that minimises a cost function $J(\boldsymbol{x}, \boldsymbol{u})$, where $\boldsymbol{x}$ and $\boldsymbol{u}$ are vectors of system states and control signals, respectively. Optimal control combination is referred to as $\boldsymbol{u}^*(\boldsymbol{x})$. Mathematically stated as

$$\begin{aligned} \boldsymbol{u}^*(\boldsymbol{x}) = \operatorname{argmin}_{\boldsymbol{u}\in U} J(\boldsymbol{x}, \boldsymbol{u}) \\ \text{subject to } |\dot{\boldsymbol{u}}| < \dot{\boldsymbol{u}}_{\max} \end{aligned}, \tag{1}$$

where U is a set of all admissible actuator commands and $\dot{\boldsymbol{u}}_{\max}$ is a vector that defines the maximum values of the rate of change of the control commands. The values for $\dot{\boldsymbol{u}}_{\max}$ can be determined based on actuator dynamics. Absolute and comparison operators in Equation (1) act element wise. The cost function $J(\boldsymbol{x}, \boldsymbol{u})$ consists of components related to fuel economy and estimated velocity error of the system. Because the controller optimises the cost for one sample interval at a time, the cost has to be power type, instead of energy. Therefore, the first component is the estimated consumption per travelled distance. One sample interval optimisation is also referred as instantaneous optimisation (Paganelli *et al.* 2000). The results obtained with this method will be restricted to local optimality. The costs are evaluated with

$$J(\boldsymbol{x}, \boldsymbol{u}) = q_1 \frac{\hat{\dot{m}}_f(\boldsymbol{x}, \boldsymbol{u})}{\hat{v}(\boldsymbol{x}, \boldsymbol{u})} + q_2 \left| v_{\text{ref}} - \hat{v}(\boldsymbol{x}, \boldsymbol{u}) \right| \tag{2}$$

where q_1 and q_2 are weighting coefficients, v_{ref} is the velocity reference, $\hat{\dot{m}}_f(\boldsymbol{x}, \boldsymbol{u})$ and $\hat{v}(\boldsymbol{x}, \boldsymbol{u})$ refer to the estimated mass flow of fuel and velocity, respectively. In actual implementation, we will translate actuator constraints $|\dot{\boldsymbol{u}}| < \dot{\boldsymbol{u}}_{\max}$ to penalising $|u(t) - u(t-i)|$, for $i = 1, 2, 3$.

2.2.2. System model

In the previous section, we defined a cost function that requires estimating the fuel consumption and velocity of the machine. In this section, we derive appropriate equations that can be evaluated with measured variables of HSD and show how the cost is calculated. The interactions of the system components are presented in Figure 3. The figure also shows the control commands of the engine $n_{e,\text{com}}$, HSD pump $\varepsilon_{p,\text{com}}$ and motors $\varepsilon_{m,\text{com}}$, entering to the diagram from the top. All these 3 inputs have an effect on the velocity of the machine v (output) (see Equation (5)). The control vector of the research platform is therefore defined by $\boldsymbol{u} = \begin{bmatrix} n_{e,\text{com}} & \varepsilon_{p,\text{com}} & \varepsilon_{m,\text{com}} \end{bmatrix}$.

To overcome the load forces F_L, the pressure difference $\Delta p = p_B - p_A$ over the hydraulic motors has to be high enough. The pump provides flow Q_p that both pressurises the volumes A and B (see Figure 3), and determines the rotational speed of the motors. This eventually defines the torque exerted on the engine (see Equation (4) for T_e). In steady-state conditions, i.e. $\dot{\boldsymbol{x}} = 0$, the fuel mass flow of the engine $\dot{m}_f(\boldsymbol{x})$ depends on its output power $P_e(\boldsymbol{x})$ and efficiency. The latter is commonly described with BSFC, which states how much fuel has to be injected in order to produce a unit of energy. The fuel consumption of engine can be calculated with

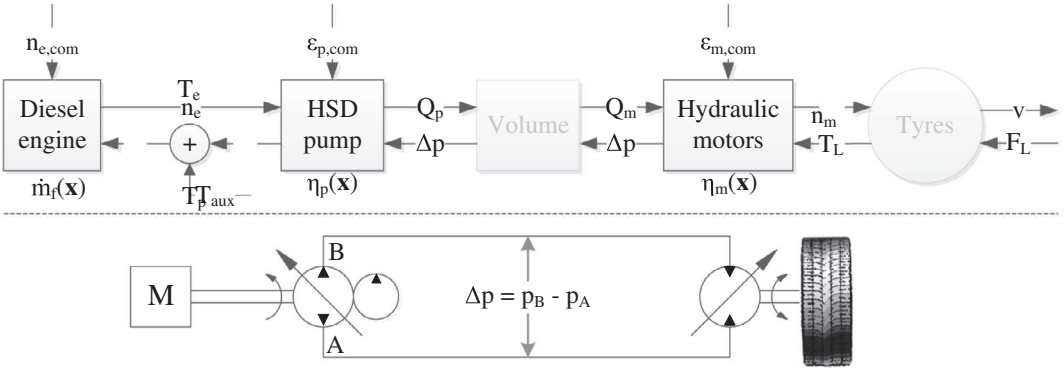

Figure 3. Interactions of HSD components.

$$\begin{aligned}\dot{m}_f(\boldsymbol{x}) &= P_e(\boldsymbol{x}) \times BSFC\left(T_e(\boldsymbol{x}), n_e\right) \\ &= 2\pi n_e T_e(\boldsymbol{x}) \times BSFC\left(T_e(\boldsymbol{x}), n_e\right)\end{aligned} \tag{3}$$

From the variables of Equation (3), rotational speed of the engine is easy and inexpensive to measure. However, measuring the torque $T_e(\boldsymbol{x})$ requires sensors not applicable for cost-conscious machine manufactures. Therefore, the required torque has to be calculated with

$$T_e(\boldsymbol{x}) = T_p(\boldsymbol{x}) + T_{\text{aux}}(\boldsymbol{x}) = \frac{\varepsilon_p V_p \Delta p}{2\pi \eta_{\text{hm},p}(\boldsymbol{x})} + T_{\text{aux}}(\boldsymbol{x}), \tag{4}$$

where $T_p(\boldsymbol{x})$ and $T_{\text{aux}}(\boldsymbol{x})$ denote the required torques of HSD pump and auxiliary devices, respectively. Here auxiliary devices include e.g. boost pump (see Figure 2), hydraulic steering pump and charger. Δp is the pressure difference over the HSD pump and motors. $\eta_{\text{hm},p}(\boldsymbol{x})$ represents the hydromechanical efficiency of HSD pump. This variable includes mechanical losses such as frictions.

The other variable required in the cost function (Equation (2)) is the velocity of machine $v(\boldsymbol{x})$. For the HSD of the research platform, this can be calculated with

$$\begin{aligned}v(\boldsymbol{x}) &= \overbrace{\frac{d_t}{2} 2\pi \frac{n_m}{60}(\boldsymbol{x})}^{Q_p} \\ &= d_t \pi \, V_p \varepsilon_p \frac{n_e}{60} \eta_{\text{vol},p}(\boldsymbol{x}) \, \frac{\eta_{\text{vol},m}(\boldsymbol{x})}{4 V_m \varepsilon_m},\end{aligned} \tag{5}$$

where d_t is the diameter of the tyre, n_m is the rotational speed of the motor, $\eta_{\text{vol},p}(\boldsymbol{x})$ and $\eta_{\text{vol},m}(\boldsymbol{x})$ are volumetric efficiencies of HSD pump and motors, respectively. This efficiency accounts for volumetric losses, for example leakages.

In order to determine the optimal control combination $\boldsymbol{u}^*(\boldsymbol{x})$, we need to know the loading conditions of the machine. At constant speed, i.e. $\dot{v} = 0$, they are defined only by load torque $T_L = F_L \frac{d_t}{2}$ (see Figure 3), namely frictions, the effect of gravity, air resistance etc. Therefore, as Δp can be measured, we are able to calculate T_L with

$$m\hat{v} = \frac{T_m - T_L}{\frac{d_t}{2}} \overbrace{\Rightarrow}^{\hat{v}=0} T_L = \varepsilon_m \frac{V_m}{2\pi} \Delta p \eta_{\text{hm},m}(\boldsymbol{x}), \tag{6}$$

where T_m and $\eta_{\text{hm},m}(\boldsymbol{x})$ are the torque and hydromechanical efficiency of the HSD motors, respectively. The same equation is also used to estimate Δp for the other ε_m, having estimated T_L. Details are presented in Section 3.2.

In this paper, we need the following simplifying assumptions on the system operation:

- Pressure loss and leakage of the hoses are considered insignificant i.e. $\Delta p_p = \Delta p_m$ and $Q_p = Q_m$.
- No slip or slide of the wheels (See Equation (5)).
- Temperature/viscosity is assumed constant, that is, we assume it does not have an effect on hydraulic efficiencies.
- Load torque remains unchanged regardless of v_{ref} changes for the next control cycle.

3. Controller implementation

The purpose of the devised controller is to improve the fuel economy of the HSD, while preserving the controllability of the system and tracking the velocity reference of the operator. This is achieved by selecting the optimal control combination $\boldsymbol{u}^*$ based on Equation (1). Recall that $\boldsymbol{u}^*$ includes the optimal control commands of the engine $n^*_{e,\text{com}}$, HSD pump $\varepsilon^*_{p,\text{com}}$ and motors $\varepsilon^*_{m,\text{com}}$.

The hydraulic efficiencies of HSD pump (see Equations (4) and (5)) are estimated based on steady-state laboratory measurements. The estimates of BSFC of the engine (see Equation (3)) and the efficiencies of HSD motors (see Equations (5) and (6)) are based on the data provided by their manufacturers.

3.1. Structure of controller

Figure 4 presents the block diagram of the main parts of the controller. The inputs of the controller are v_{ref}, Δp, n_e, ε_p and ε_m. For numerical calculation purposes, we discretize the control space. The set of discrete admissible control commands is then called

U_D, $U_D \subset U$. U_D is defined by

- U_e:{1000, 1010, … , 2200} r/min,
- U_p:{0, 0.01, … , 1} and
- U_m:{0.5, 1},

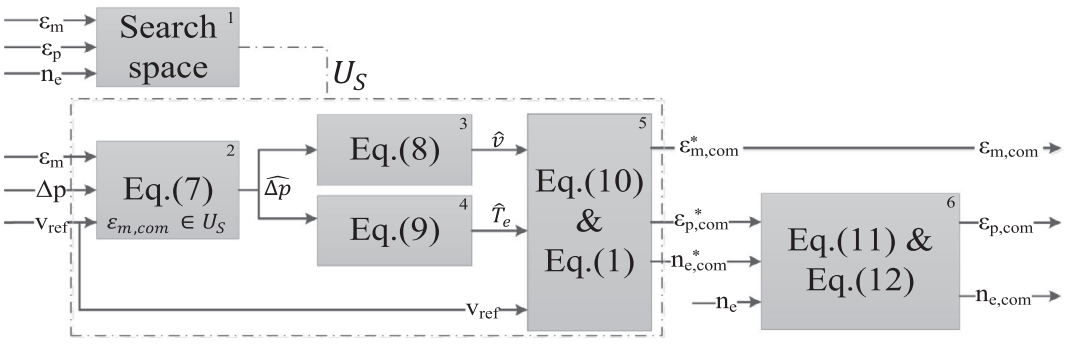

Figure 4. Implementation structure of the optimal controller.

i.e.

$$U_D = U_e \times U_p \times U_m = \left\{ \left(n^*_{e,\mathrm{com}}, \varepsilon^*_{p,\mathrm{com}}, \varepsilon^*_{m,\mathrm{com}} \right) \middle| n^*_{e,\mathrm{com}} \in U_e, \varepsilon^*_{p,\mathrm{com}} \in U_p, \varepsilon^*_{m,\mathrm{com}} \in U_m \right\}.$$

This choice was made to improve calculation efficiency and to match U_D to the resolution of the CAN interface. However, optimisation search space is reduced to U_S, a subset of U_D. Details are defined in Section 3.5. This is depicted in Block 1, Figure 4. These choices enable the implementation of the controller also to control units with significantly lower calculation power e.g. commercial PLCs.

In Block 2, first the loading condition is estimated. In Block 3 and 4, machine velocities and required engine torques for every control combination are calculated (with the discretization choices U_D includes $121 \times 101 \times 2 = 24,442$ combinations in total). Finally, in Block 5, the optimal control combination is calculated (see Equation (12)) and transmitted to the actuators. Block 6 is added for controllability, to be detailed in Section 3.6. Obviously, consumption optimisation is as accurate as the accuracy of the models allow. The cycle time of the optimisation t_{opt} (Figure 4 blocks 1–5) is 48 ms. In the next few sections, each block is presented in detail.

3.2. Load estimation

This section describes Figure 4, block 2. Restating Equation (6) in terms of the systems states, we have $\widehat{T}_L = \frac{V_m}{2\pi} \hat{\eta}_{\mathrm{hm},m}\left(n_{m,\mathrm{ref}}, \varepsilon_m, \Delta p\right) \varepsilon_m \Delta p$. We can see that if the motor displacement remains the same, constant load assumption translates to constant pressure Δp. Thus for forthcoming blocks, we will use Δp to represent the load and all we need to do is to estimate Δp for all feasible motor displacements. However, given ε_m solving above equation for Δp is rather complex. We thus approximately solve it based on the observation that for relatively flat efficiency curve (based on measurement data) the pressure change will be proportional to the motor displacement change, that is, $\varepsilon_m / \varepsilon_{m,\mathrm{com}} \Delta p$ will be used to estimate hydromechanical efficiency of HSD motors $\hat{\eta}_{\mathrm{hm},m}$. Putting all together, we can write

$$\widehat{\Delta p} = \frac{\widehat{T}_L}{\hat{\eta}_{\mathrm{hm},m} \frac{V_m}{2\pi} \varepsilon_{m,\mathrm{com}}} = \frac{\hat{\eta}_{\mathrm{hm},m}\left(n_{m,\mathrm{ref}}, \varepsilon_m, \Delta p\right) \varepsilon_m}{\hat{\eta}_{\mathrm{hm},m}\left(n_{m,\mathrm{ref}}, \varepsilon_{m,\mathrm{com}}, \frac{\varepsilon_m}{\varepsilon_{m,\mathrm{com}}} \Delta p\right) \varepsilon_{m,\mathrm{com}}} \Delta p, \forall \varepsilon_{m,\mathrm{com}} \epsilon U_S \tag{7}$$

where $n_{m,\mathrm{ref}} = 60 v_{\mathrm{ref}} / \left(\pi d_t\right)$. Notice that estimated pressure difference $\widehat{\Delta p}$ for the current ε_m is simply the same as the measured Δp.

In Equation (7), $\hat{\eta}_{\mathrm{hm},m}$ is estimated based on manufacturer data as a function of rotational speed, motor displacement and pressure difference. Since we assume that load remains unchanged and perform the calculations in steady-state, it is better to low pass filter Δp before utilization to reduce its high dynamic components. A modified version of the filter engineered by Luomaranta (1999) is utilized for this purpose.

3.3. Steady-state velocity and torque estimates

Having calculated the pressure differences for both $\varepsilon_{m,\mathrm{com}}$ with Equation (7), it is possible to calculate the velocity of the machine and the required output torque of the engine with Equations (5) and (4), respectively. This section describes how these variables are estimated for all 24,442 control combinations.

3.3.1. Machine velocity estimates

This section describes Figure 4, block 3. Equation (5) determines the velocity of the machine as a function of $\eta_{\mathrm{vol},p}$ and $\eta_{\mathrm{vol},m}$. Replacing the coefficients with their estimates in Equation (5), we have

$$\hat{v} = \pi d_t \frac{V_p}{V_m} \frac{n_{e,\mathrm{com}}}{60} \frac{\varepsilon_{p,\mathrm{com}}}{\varepsilon_{m,\mathrm{com}}} \hat{\eta}_{\mathrm{vol},p}\left(n_{e,\mathrm{com}}, \varepsilon_{p,\mathrm{com}}\right) \hat{\eta}_{\mathrm{vol},m}\left(n_{m,\mathrm{ref}}, \varepsilon_{m,\mathrm{com}}\right), \forall \left(n_{e,\mathrm{com}}, \varepsilon_{p,\mathrm{com}}, \varepsilon_{m,\mathrm{com}}\right) \epsilon U_S \tag{8}$$

To reduce computational costs, tabulated velocity estimates are used instead of calculating them again for every execution cycle. As seen from Equation (8), the effect of Δp on volumetric efficiency is not considered even though pressure is known to have a strong effect on the leakages. Instead, $\hat{\eta}_{\mathrm{vol}}$ are calculated with a Δp that corresponds a value of steady-state driving with an appropriate $\varepsilon_{m,\mathrm{com}}$. If measured pressure values were utilized, increasing Δp would result in increasing leakages (decreasing η_{vol}), which would have to be compensated by increasing Q_p. This would raise pressure even more and cause oscillations that also decrease the fuel economy of the machine. This implementation was chosen to reduce oscillations during the acceleration of the machine. However, it increases velocity reference tracking error.

3.3.2. Engine output torque estimates

This section describes Figure 4, block 4. Required Te can be calculated with Equation (4). Final estimate values $\hat{T}_e$ are determined with

$$\hat{T}_e = \begin{cases} \infty & , \widehat{T}_e > T_{e,\max}\left(n_{e,\mathrm{com}}\right) \\ \varepsilon_{p,\mathrm{com}} \frac{V_p}{2\pi} \frac{\widehat{\Delta p}\left(\varepsilon_{m,\mathrm{com}}\right)}{\hat{\eta}_{\mathrm{hm},p}\left(n_{e,\mathrm{com}}, \varepsilon_{p,\mathrm{com}}, \widehat{\Delta p}\left(\varepsilon_{m,\mathrm{com}}\right)\right)} + T_{\mathrm{aux}} & , \text{otherwise} \end{cases} \tag{9}$$

$$, \forall \left(n_{e,\mathrm{com}}, \varepsilon_{p,\mathrm{com}}, \varepsilon_{m,\mathrm{com}}\right) \in U_S$$

$\widehat{T}_e$ assumes a bounded value only if a certain control combination is feasible i.e. the maximum torque curve of the engine ($T_{e,\max}(n_{e,\mathrm{com}})$) is not exceeded. For an unfeasible combination, the required torque is set to infinity, which results in infinite cost. T_{aux} is considered constant.

Exceeding the maximum torque curve should especially be avoided when n_e is below the speed of maximum torque (usually in the middle of operation region). In this rising part of the torque curve, high load can easily stall the engine. This originates from the basic operation of diesel engines, because with constant throttle setting their rotational speed decreases when load increases. If the engine operates at this region, it will generate less torque for lower speed, thus the speed will drop even more. Eventually, this results in the stall of the engine, if the load is not reduced accordingly. This will be addressed in Section 3.6.2.

3.4. Cost function

In the cost function of Equation (2), the penalised variables included consumed fuel for travelled distance ([g/m]) and estimated velocity error. Equation (3) is utilized in the evaluation of $\widehat{m}_f$, in which BSFC is estimated based on manufacturer data.

In addition, the initial optimisation problem (see Equation (1)) was constrained with the maximum values of control command derivatives. For the investigated HSD system, this yields $|\dot{n}_{e,\mathrm{com}}| < \dot{n}_{e,\max}$, $|\dot{\varepsilon}_{p,\mathrm{com}}| < \dot{\varepsilon}_{p,\max}$ and $|\dot{\varepsilon}_{m,\mathrm{com}}| < \dot{\varepsilon}_{m,\max}$. The hard constraints $\dot{n}_{e,\max}$, $\dot{\varepsilon}_{p,\max}$ and $\dot{\varepsilon}_{m,\max}$ describe the maximum rates of change for the rotational speed of the engine and displacements of HSD pump and motors, respectively.

Approximating the control command derivatives with

$$|\dot{\boldsymbol{u}}| \approx \left| \frac{\boldsymbol{u}(t) - \boldsymbol{u}(t-1)}{t_{\mathrm{opt}}} \right| \tag{10}$$

yields

$$\frac{\dot{\boldsymbol{u}}}{\dot{\boldsymbol{u}}_{\max}} \approx \frac{\boldsymbol{u}(t) - \boldsymbol{u}(t-1)}{t_{\mathrm{opt}}\dot{\boldsymbol{u}}_{\max}} = \frac{\boldsymbol{u}(t) - \boldsymbol{u}(t-1)}{\Delta \boldsymbol{u}_{\max}} \tag{11}$$

where $\Delta \boldsymbol{u}_{\max}$ is the maximum control command change in one calculation cycle. This can be utilized in implementing the limits as soft constraints. Therefore, limit can be defined also for $|\dot{\varepsilon}_{m,\mathrm{com}}|$, which would not be otherwise applicable for motors with 2 discrete displacement settings. Our implementation defines $\dot{\varepsilon}_{m,\max}$ in terms of maximum switching frequency i.e. we penalise the number of switches made in 3 calculation cycles ($i_{\max} = 3$ in Equation (12)).

The normalised costs of feasible control combinations are evaluated with

$$\begin{aligned} J(\boldsymbol{x}(t), \boldsymbol{u}(t)) = \\ q_1 \frac{\hat{\dot{m}}_f(t)/\hat{v}(t)}{(\dot{m}_f/v)_{\max}} + q_2 \frac{|v_{\mathrm{ref}}(t) - \hat{v}(t)|}{\Delta v_{\max}} \\ + r_1 \sum_{i=1}^{i_{\max}} \frac{|\varepsilon_{m,\mathrm{com}}(t) - \varepsilon_{m,\mathrm{com}}(t-i)|}{i_{\max}\Delta\varepsilon_{m,\max}} \\ + r_2 \sum_{i=1}^{i_{\max}} \frac{|\varepsilon_{p,\mathrm{com}}(t) - \varepsilon_{p,\mathrm{com}}(t-i)|}{i_{\max}\Delta\varepsilon_{p,\max}} \\ + r_3 \sum_{i=1}^{i_{\max}} \frac{|n_{e,\mathrm{com}}(t) - n_{e,\mathrm{com}}(t-i)|}{i_{\max}\Delta n_{e,\max}} \\ , \forall \left(n_{e,\mathrm{com}}, \varepsilon_{p,\mathrm{com}}, \varepsilon_{m,\mathrm{com}} \right) \in U_S \end{aligned} \tag{12}$$

where r_1, r_2 and r_3 are weighting coefficients. In addition, $(\dot{m}_f/v)_{\max}$ and $\Delta v_{\max}$ are maximum values for consumption and velocity error, respectively. Maximum values for control command changes (i.e. $\Delta\varepsilon_{m,\max}$, $\Delta\varepsilon_{p,\max}$ and $\Delta n_{e,\max}$) are defined with search space (see Section 3.5). This results in normalised cost.

Following values have been chosen for the weighting factors: $q_1 = 0.65$, $q_2 = 0.31$, $r_1 = 0.0025$, $r_2 = 0.0095$ and $r_3 = 0.028$, which sum up to 1. The control combination that results in the lowest cost is selected as the output of the optimal controller $\boldsymbol{u}^*$ (see Figure 4, block 5).

Penalising command changes reduces e.g. pressure variations and the wear of the actuators as the changing frequency is lower. Experiments show that fuel economy is also improved. This might originate from the fact that every time n_e is increased and again decreased some amount of energy cannot be recuperated back from rotational energy.

3.5. Search space

This section describes Figure 4, block 1. The block enables the reduction of computational effort by reducing the number of investigated control combinations. This is important especially if the controller is implemented to a control unit with lower calculation power because the costs of all control combinations within the search space are evaluated in every execution.

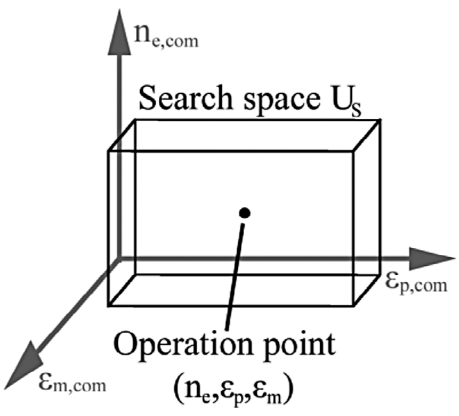

Figure 5. Search space of the optimal controller.

The size of this search space U_S can be freely defined in advance and separately for $n_{e,\mathrm{com}}$, $\varepsilon_{p,\mathrm{com}}$ and $\varepsilon_{m,\mathrm{com}}$; $U_S \subset U_D$. This facilitates successful real-time implementation. A graphical illustration is presented in Figure 5.

The following choices have been made. If the search space does not cover all the possible control combinations ($U_S \neq U_D$), evaluated combinations depend on current operation point. The number of feasible command values above and below the measured value of a control variable is independent, but their sum is always constant $\Delta \boldsymbol{u}_{\max}$. For example, if ε_p is at maximum, the number of feasible commands below the measured value is increased correspondingly. This also limits the maximum rate of change of the control variables for one evaluation cycle of the controller. With the appropriate selection of the maximum values of the control command changes, the constraint of Equation (1) can be fulfilled as $|\dot{\boldsymbol{u}}| \leq \Delta \boldsymbol{u}_{\max}/\Delta t_c < \dot{\boldsymbol{u}}_{\max}$.

This has an effect on the functionality of the machine in a similar way as the costs of the command changes in Equation (12). In practice, $\hat{T}_e(\boldsymbol{u}) = \infty, \boldsymbol{u} \notin U_S$, i.e. if a control combination is outside the search space, it is made unfeasible by setting the corresponding torque to infinity. This is similar to the case where maximum torque value is exceeded in Equation (9).

3.6. Additional parts of the controller for improved functionality

Because the optimal controller utilizes only the steady-state equations of the system, some additional strategies are implemented to improve controllability. Firstly, engine droop is compensated by increasing the $n^*_{e,\mathrm{com}}$, according to the estimated load. Secondly, the load of the engine is limited by limiting the $\varepsilon^*_{p,\mathrm{com}}$. Both are evaluated every time the inputs of the controller are acquired, i.e. at 4-ms cycle. The faster cycle time (compared to optimisation) enables more rapid reactions for the changes of load (see Figure 4, block 6).

In addition, the rate of change of $\varepsilon_{p,\mathrm{com}}$ has to be limited during motor displacement change and $\varepsilon_{m,\mathrm{com}}$ is set to 1 in the high loading conditions of HSD. Both of these features reduce the unwanted switching of $\varepsilon_{m,\mathrm{com}}$, which oscillates also other control commands.

3.6.1. Feedforward to compensate engine droop

The electronic control units of diesel engines have closed loop control for rotational speed. However, usually a certain amount of error is allowed. This is called engine droop and it is proportional to the load of the engine. Droop dampens the response and stabilizes engine controller. For example, with $n_{e,\mathrm{com}}$ = 1000 r/min and 5% maximum droop, $n_{e,\mathrm{com}}$ will be 950 r/min in full load condition. In governor controlled diesel engines, droop is determined with the spring rate of governor.

When $\boldsymbol{u}^*$ is determined based on the model of the machine, $n^*_{e,\mathrm{com}}$ (i.e. the optimal point) cannot be reached without compensating engine droop. This is done with a feedforward compensator implemented with

$$n_{e,\mathrm{com}} = \left(1 + K_{\mathrm{droop}} \frac{\hat{T}_e(\boldsymbol{u}^*)}{T_{e,\max}\left(n^*_{e,\mathrm{com}}\right)}\right) n^*_{e,\mathrm{com}} \,, \tag{13}$$

where K_{droop} is a parameter that defines maximum droop value ($\left[K_{\mathrm{droop}}\right] = \%$). The compensator increases $n^*_{e,\mathrm{com}}$ based on estimated load torque ($\hat{T}_e(\boldsymbol{u}^*)$) and parameter K_{droop}. As a result, the compensated command $n_{e,\mathrm{com}}$ should decrease the error between the measured n_e and the optimal command $n^*_{e,\mathrm{com}}$.

3.6.2. Limiting fast load

The optimal controller is only valid for quasi-static situations, because of the models used. The bandwidth of the controller is also limited by low-pass filtering the measured Δp. To address fast dynamic situations, e.g. when the machine is driven to a hill or accelerated rapidly, the maximum displacement command of the HSD pump is limited to a value $\varepsilon_{p,\mathrm{com}}$ to restrict load on the engine. Otherwise, fast load transient might stall the engine. The displacement of HSD pump is limited with

$$\varepsilon_{p,\mathrm{com}} = \begin{cases} \varepsilon^*_{p,\mathrm{com}} & , n^*_{e,\mathrm{com}} - n_e \leq K_{\mathrm{droop}} n^*_{e,\mathrm{com}} \\ \min\left(\varepsilon_{p,\max} - \frac{\min\left(n^*_{e,\mathrm{com}} - n_e, \Delta n_{e,\max}\right)}{\Delta n_{e,\max}}, \varepsilon^*_{p,\mathrm{com}}\right) & , \text{otherwise} \end{cases} \tag{14}$$

where $\varepsilon_{p,\mathrm{com}}$ is the command value send to the pump, and $\varepsilon_{p,\max} = 1$ is the maximum displacement of the HSD pump. The condition on the first row is equivalent to maximum allowed engine droop for maximum available torque, see Equation (11). In the second row, that is, when the engine speed error $n^*_{e,\mathrm{com}} - n_e$ is too high, pump displacement is reduced proportional to the engine speed error and a maximum allowed error $\Delta n_{e,\max}$. Notice that if $n^*_{e,\mathrm{com}} - n_e \geq \Delta n_{e,\max}$, then $\varepsilon_{p,\mathrm{com}} = 0$. Additionally, this function facilitates accelerating the rotational speed of the engine, because of increased available torque and the engine operating in regions with better dynamic characteristics. Notice that in Equation (14), $n^*_{e,\mathrm{com}}$ is used instead of $n_{e,\mathrm{com}}$ not including the inverse function of Equation (13) when limiting the ε_p.

3.6.3. Rate limiter for pump command during motor displacement change

In simulation studies reported in (Backas *et al.* 2014), motor dynamics were not considered. However, in the real machine, motor displacement change has considerable dynamic (approximately 300 ms from 50 to 100%). We need to synchronise the pump displacement and that of the motor. This has dramatic effect on the performance of the control system since motor displacement

is discrete, and thus causes large changes in speed and pressures. Different ramp functions are used for increasing and decreasing motor commands.

This feature evidently prevents optimal control commands reaching the actuators while active.

3.6.4. Feasible motor displacements at a steep uphill

The manufacturer of the HSD pump has included a function that limits the ε_p when p_B or p_A exceeds a predefined limit. This feature, called pressure cut-off, was not included in the simulation model of the machine utilized in the experiments of Backas *et al.* (2014) yet in the real machine it has a dramatic effect on performance near maximum pressure.

When pressure increases too high, for example at a steep uphill, ε_p decreases due to pressure cut-off, but as soon as the corresponding pressure (p_B in forward motion) drops, ε_p is increased again. This leads to oscillations in the displacement of the HSD pump and pressures in this kind of situations. More importantly, because $\boldsymbol{u}^*$ is determined based on Δp, motor command $\varepsilon^*_{m,\mathrm{com}}$ starts to oscillate between 0.5 and 1 values, further degrading the performance of the machine. To prevent the described phenomenon, we set the displacement of hydraulic motor to full (i.e. $\varepsilon_{m,\mathrm{com}} = 1$), when Δp exceeds 300 bars. Reduced displacement is again enabled when $\Delta p < 80$ bars, for example when the machine has reached the hill top.

4. Architecture

The computer running the compiled Simulink code in xPC Target environment has 2.53 MHz Intel Core i7 CPU with 2 GB RAM (see QM-57 in Figure 6). The collected data is saved with 2-ms sample time to a 16 GB SSD drive before downloading it after every experiment.

The computer is connected to three of the four main CAN buses of the machine. Currently, all data related to the engine, e.g. the control command $n_{e,\mathrm{com}}$ and the measured speed n_e, is transmitted to a commercial control unit BODAS RC36 by Bosch Rexroth which forwards them to appropriate buses. The architecture of HSD control hardware is presented in Figure 6.

The outputs of the optimal controller are first send to RC36, which transmits them to the HSD actuators.

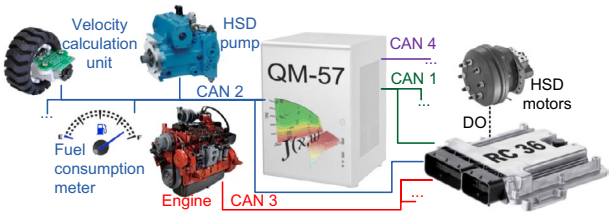

Figure 6. Architecture of HSD control hardware.

This guarantees isochronous transmission of control commands and facilitates implementing safety features, because all commands can be reset in one unit.

5. Real-world experiments

The optimal controller was initially developed in a real-time simulator. The controller was implemented in similar xPC Target environment that is used also in the real machine. The simulation results are presented in Backas *et al.* (2014), where a constant rotational speed controller was used as baseline.

Presented tests include only driving, but the controller can also be utilized as a part of the control system of the entire machine that has a client–server structure described in Ahopelto *et al.* (2012). This does not have an effect on the results if the power of HSD is not limited e.g. due to the operation of implement hydraulics.

5.1. Description of the tests & testing area

The experimental tests were conducted with the wheel loader described in Section 2.1 in the testing area of IHA. Figure 7 presents an overview of the site.

In this paper, two different kinds of tests are presented to evaluate the efficacy and functionality of the devised optimal controller.

Test 1. Improved fuel economy is verified by driving autonomously around the area along the multicolour path described in Figure 7. This test includes both asphalt (flat:red and uphill:blue) and gravel (downhill:green and flat:magenta) sections. Velocity reference for the red and blue parts (flat) is 4 m/s, for the green (downhill) 1 m/s, and for the magenta part (flat) 2 m/s. The machine starts from standstill at every lap at the point marked with the black X. Autonomous control of a similar machine is described in (Ghabcheloo *et al.* 2009).

Test 2. In addition, in a second test scenario, the functionality of the controller is demonstrated in hill climbing tests, in which the machine is driven along straight path (see orange arrow in Figure 7) to such a steep hill that without initial kinetic energy, its climbing capacity would be insufficient. This test is conducted with constant velocity references 4, 5 and 6 m/s.

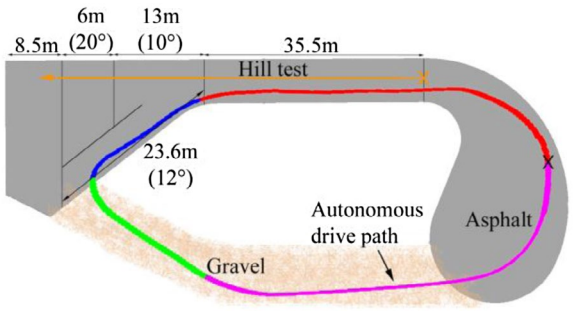

Figure 7. Overview of the testing area with the paths of hill and autonomous tests.

5.2. Rule-based controller

The optimal controller is compared to a rule-based controller that is very similar to algorithms used in commercial wheel loaders (Bosch Rexroth AG 2003, Korane 2004, Eaton Corporation 2007). Algorithms resulting to global optimality e.g. dynamic programming (DP) were not utilized here, because they require knowledge about the complete cycle. In empirical testing, gathering this data is not a trivial matter.

Optionally, DP could be utilized as benchmark with a pure simulation experiment. However, all simulation models include assumptions and simplifications which would cause uncertainty to the results. For example, consumption of engine in transient situations is uncertain to model. Moreover, the focus of this research is to demonstrate real measured fuel economy benefits, and therefore simulations were excluded.

The most widely used HSD structure for wheel loaders has one variable displacement hydraulic motor and mechanical drive shafts. The 2-speed hub motors installed in our research platform are rarely utilized. For these reasons, our rule-based controller is not identical to commercial algorithm, but their main principles are the same.

Figure 8 presents how the control commands are determined. The velocity reference of operator sets directly the command of the engine $n_{e,\mathrm{com}}$ as shown in Figure 8. Immediately after v_{ref} exceeds a minimum value, $n_{e,\mathrm{com}}$ is increased from idle speed to 1100 r/min. After this, the engine command is directly proportional to v_{ref}. With 5-m/s reference, $n_{e,\mathrm{com}}$ is set to 1650 r/min. The displacements of the hydraulic components are set based on measured and filtered engine speed n_e (not $n_{e,\mathrm{com}}$) using a function visualized in the middle and right hand side plots.

As stated above, rules of the controller are based on commercial algorithms and it is tuned to minimise the steady-state velocity error of the machine on level ground. It is clear that the rules can be changed to achieve better fuel economy, but then it would not correspond to the mentioned widely used hydromechanical controllers.

If the hydraulic motor was variable displacement type, $\varepsilon_{m,\mathrm{com}}$ would be decreased as $\varepsilon_{p,\mathrm{com}}$ increases. With 2-speed motors, the point where $\varepsilon_{m,\mathrm{com}}$ changes from 1 to 0.5 is problematic when it is set based on engine speed. This is because it can easily start switching up and down as the engine load depends on pump displacement according to Equation (4) and n_e varies based on the load. For this reason, we have implemented a hysteresis to avoid oscillation around this region. This is presented with parallel arrows in the middle and lower plot of Figure 8. Even though this type of algorithm would not be ideal for controlling the machine, it provides better baseline for fuel economy than e.g. a controller that uses constant (or even maximum) $n_{e,\mathrm{com}}$ throughout the velocity range.

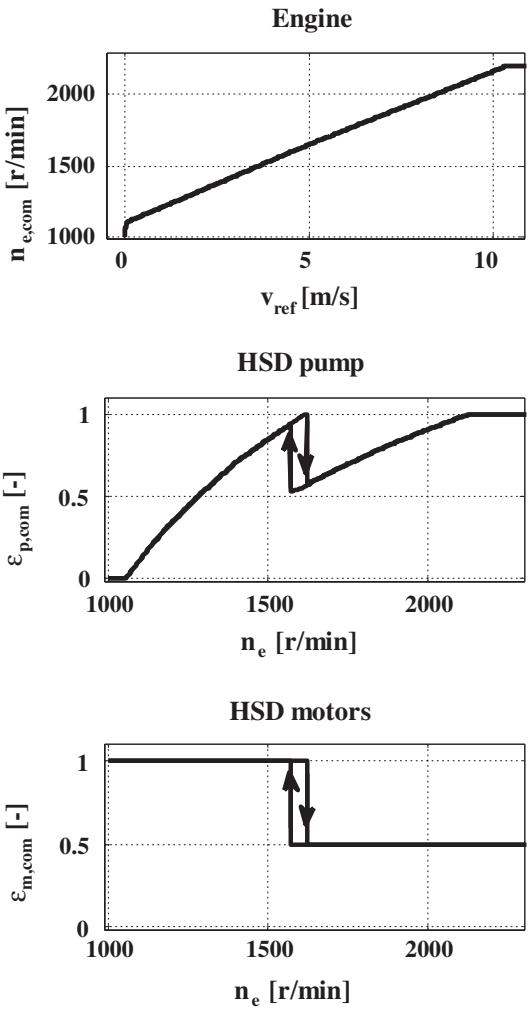

Figure 8. Control commands of the baseline controller.

In addition to the rules above, $\varepsilon_{m,\mathrm{com}}$ is set to 1 if filtered Δp exceeds 300 bars; setting $\varepsilon_{m,\mathrm{com}} = 0.5$ is again enabled when Δp falls below 80 bars. This maximises the climbing capacity of the machine and prevents unintended switching of the control command. This control rule is similar to the one of the optimal controller described in Section 3.6.4.

5.3. Results

Figure 9 presents measured fuel consumption for five different velocities at steady-state situation for both controllers. In all the figures of this section, rule-based and optimal controllers are referred as RB and OPT, respectively.

As shown in Figure 9, the optimal controller provides drastic improvements to the fuel efficiency in steady-state driving. The consumption is decreased at least 22.7% and up to 46.9% compared to the rule-based controller. In the presented measurement pairs, the velocity of the machine is not exactly the same with both controllers. For this reason, the consumption is presented by litres per 100 km. Recall that consumption per travelled distance was in the cost for optimisation. As explained

in Section 5.1, the fuel economy improvements of the optimal controller were demonstrated by driving 3 times around the test area along the path in Figure 7. The same test was conducted with and without load; a 1000-kg load was used. Subplots of Figure 10 present an approximate altitude profile of the driven path (GPS data), the measured velocity, control commands and fuel consumption of the machine. One should notice that the horizontal axis of the figure is distance instead of time. This choice was made to ease the comparison between the controllers, because now the changes occur at the same point of the horizontal axis. However, the presented consumption values (ml/m) are uncertain during transient states as velocity (m/s) and consumption (ml/s) data are not synchronised. Nevertheless, the accuracy of total amounts of fuel consumed in each test (see m_f values in Table 1) is not compromised because they are integrated values of KMA mobile (see Section 2.1.3) according to time. The curves of Figure 10 describe only a single lap around the area.

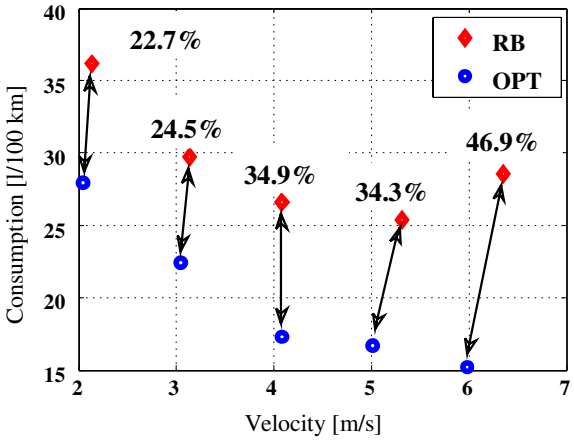

Figure 9. Steady-state consumptions with the rule-based and optimal controllers.

The optimal controller accelerates the machine by increasing the engine speed to 1350 r/min and pump displacement to 99% during the first 7 m. After this, it reduces the motor displacement to 50%. At the same time, the commands of the engine and pump are also reduced, because required volumetric flow is lower. During this steady-state phase, rule-based controller uses almost 500 r/min higher engine speed. Lower n_e leads to lower power consumption (due to constant T_{aux}). Therefore, fuel economy is improved with the optimal controller.

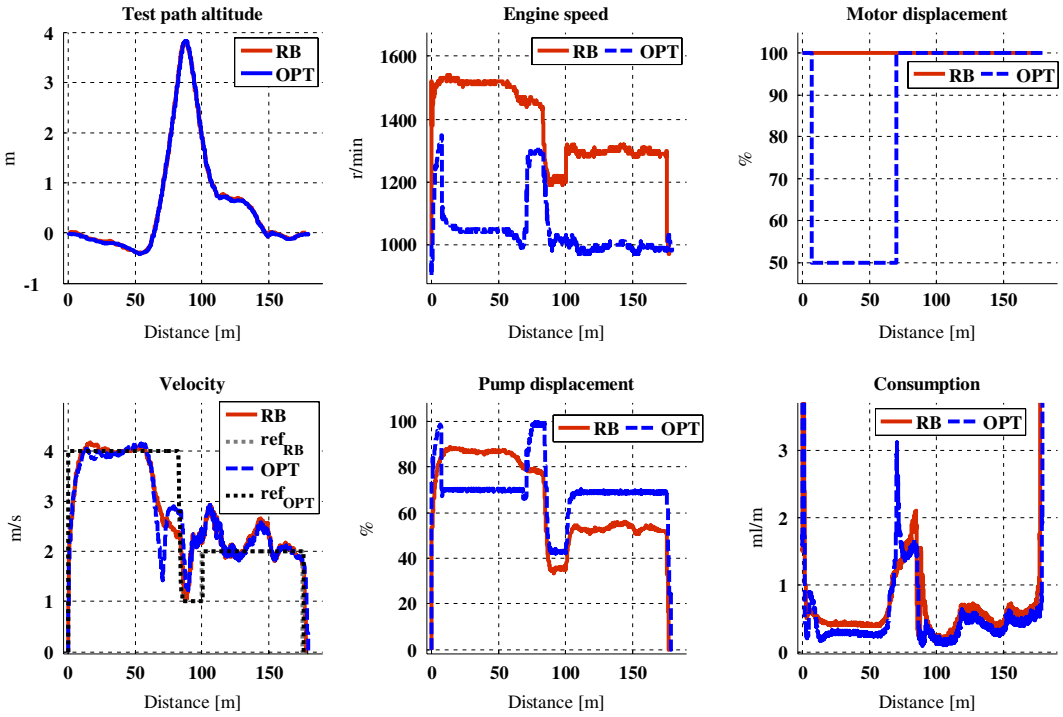

Figure 10. Autonomous drive test around the test area without load.

Table 1. Comparison of fuel consumptions in all tests.

		Optimal controller					Rule-based controller			
Test	Mass [kg]	Time [s]	m_f [ml]	Distance [m]	Cons. [ml/m]	Δcons. [%]	Time [s]	m_f [ml]	Distance [m]	Cons. [ml/m]
Autonomous drive	5000	229.3	290.4	550.9	0.53	**−16.6**	228.7	346.5	548.1	0.63
	6000	235.4	329.4	538.8	0.61	**−12.4**	233.6	375.5	538.2	0.70
Hill, 6 m/s	5000	23.8	72.9	71.9	1.01	**0.6**	21.7	70.4	69.8	1.01
Hill, 5 m/s	5000	24.4	65.1	72.3	0.90	**−0.9**	21.9	63.0	69.3	0.91
Hill, 4 m/s	5000	29.6	73.2	70.6	1.04	**8.4**	26.3	68.4	71.4	0.96

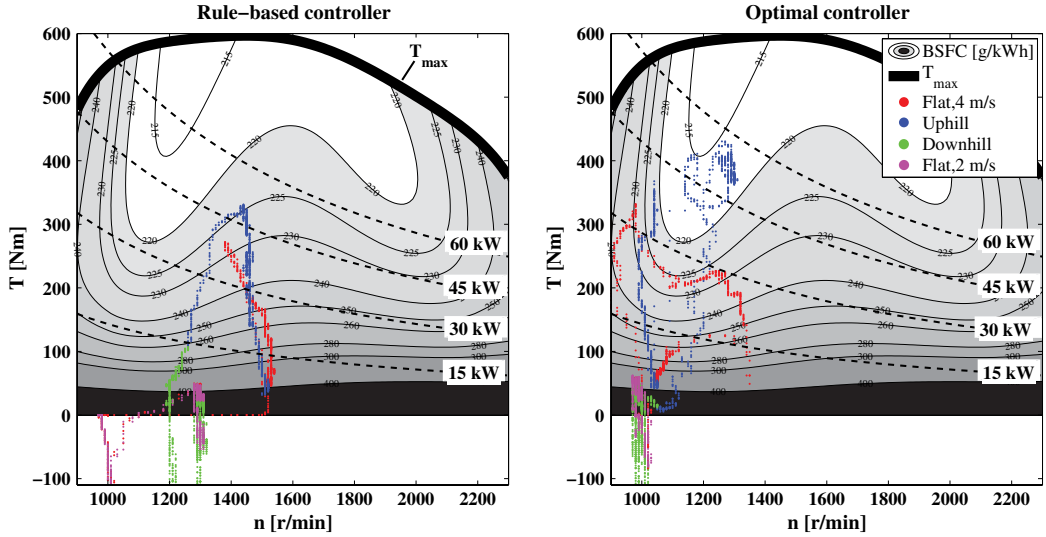

Figure 11. Operation points of the engine in the autonomous drive test without load.

However, as the machine reaches uphill, the torque generated by the hydraulic decreases rapidly with the optimal controller. Because of this, $\varepsilon_{m,\mathrm{com}}$ is increased, which requires also higher $\varepsilon_{p,\mathrm{com}}$ and $n_{e,\mathrm{com}}$. Accelerating the engine under high load (uphill) requires substantial fuel injection rate. It is evident that the resulting efficiency is momentarily below the one of the rule-based controller. Recall that the engine rotation is already higher in rule-based control.

At the downhill, both controllers exceed the 1-m/s velocity reference and their consumption is the same. In flat gravel ($v_{ref} = 2\ m/s$), the fuel economy of the optimal controller is again notably better than the one reached with the rule-based controller. As both the controllers set ε_m to 100%, this difference originates from the higher ε_p (better efficiency) and lower n_e chosen by the optimal controller. Figure 11 describes the engine operation points $\left(n_e, \hat{T}_e\right)$ in the same autonomous drive test plotted on top of the BSFC map of the engine. Same colours are used to mark different parts of the path in Figure 7. In these plots, engine torque ($\hat{T}_e$) is calculated based on measured Δp and Equation (4). In addition, curves indicating constant powers 15, 30, 45 and 60 kW are shown.

It can be seen from Figure 11 that the BSFC values of the engine are lower (i.e. lighter regions, better fuel economy) and regions with low rpm are used with the optimal controller. This is particularly clearer on flat ground with v_{ref} = 4 m/s (red points), when the lower $\varepsilon_{m,\mathrm{com}}$ results in higher $\hat{T}_e$ and lower BSFC. Moreover, in this part of the path, maximum engine powerwith the optimal and rule-based controllers are 34 and 40 kW, respectively. On the other hand, in uphill, the same value for the optimal controller is 57 kW and for the rule-based controller 50 kW.

In *Test 2* series, the functionality of the controllers was evaluated with an extreme test where the machine was driven to a hill that it cannot climb without initial speed. These tests were conducted without load. Velocity reference was kept constant during the tests. Figure 12 presents the same variables as Figure 10 with the exeption that fuel consumption is replaced with pressure difference and horizontal axis, contrary to the previous plots, is time instead of distance. This facilitates investigating the functionality of the controllers.

During the acceleration phase, the optimal controller increases the n_e to 1960 r/min and ε_p to 100%. The rule-based controller chooses slightly lower engine speed, and reduces the $\varepsilon_{m,\mathrm{com}}$ to 50% at time 3.3 s. Up to this point, the acceleration of the machine is the same with both controllers, but acceleration naturally decreases together with ε_m.

At time 4.4 s, the optimal controller reduces $\varepsilon_{p,\mathrm{com}}$, but keeps it only for 0.5 s as it decides to change the $\varepsilon_{m,\mathrm{com}}$ to 50%. This is because the controller does not predict the system behaviour or plan the future controls at all.

When the machine enters the hill (at time 10 s), both controllers have $\varepsilon_{m,\mathrm{com}}$ = 50%, which does not provide enough torque to reach the top. Therefore, $\varepsilon_{m,\mathrm{com}}$ is changed in the middle of the hill. Now more flow is needed and also other command values have to be increased. The optimal controller increases $n_{e,\mathrm{com}}$, because the high value of Δp implies high power demand. On the contrary, the rule-based controller changes $\varepsilon_{p,\mathrm{com}}$, since its $n_{e,\mathrm{com}}$ is only based on velocity reference.

The most demanding situation occurs when Δp reaches the pressure cut-off limit of the HSD pump. When activated, the pressure cut-off reduces ε_p as long as Δp exceeds the limit. This dynamic behaviour is not considered in either controller, and it causes severe oscillation in the steepest part of the hill. The optimal controller is even more sensitive to this, because it utilizes measured pressure values in calculations. Constantly changing $\varepsilon_p$results in alternating pressures which eventually causes also unwanted $n_{e,\mathrm{com}}$ changes.

Table 1 summarises the fuel consumptions of all the conducted tests. As stated earlier, *Test 1* series shows

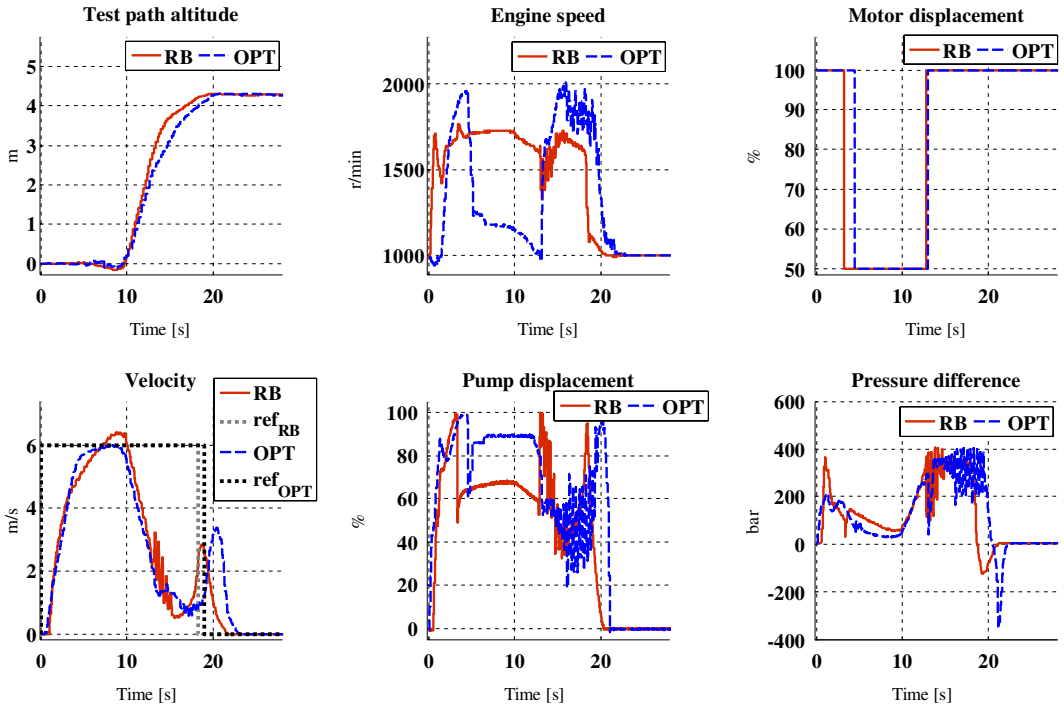

Figure 12. Hill test with constant velocity reference of 6 m/s.

fuel economy of the optimal controller compared to the rule-based, and *Test 2* series is designed to demonstrate the functionality of the controllers in extreme situation. As reference drive cycles for NRMM are not available, *Test 1* demonstrates typical transport drive situations of wheel loaders. In *Test 1* series (autonomous drive tests), measured fuel economy improvement with the optimal controller is 16.6% without load and 12.5% with 1000-kg load. See the boldface column ($\Delta cons.$) of Table 1 for the relative consumption differences of all conducted tests. Main reason why these values differ is the uphill. When the machine is heavier, more fuel has to be injected to generate enough torque with the engine.

The optimal controller uses lower rotational speeds especially in flat surface and therefore, n_e has to be increased dramatically in uphill. This deteriorates the fuel efficiency even more with load. In addition, when looking at the BSFC-map of the engine (see Figure 11), it is clear that decreasing the n_e with high constant power (e.g. 60 kW) does not improve BSFC as much as it would with lower power (e.g. 15 kW).

Even though *Test 2* series (the hill climbing tests) mainly demonstrates the functionality of the controllers, Table 1 includes also the consumed fuel amounts of steady-state situations (see Figure 9), the extreme hill tests show that the optimal controller cannot reach the lowest consumption in dynamic situations. In fact, when climbing the hill with 4-m/s reference, it consumed 8.4% more fuel than the rule-based controller. This is mainly due to the fact that the rule-based controller keeps the displacement of the hydraulic motors full throughout the test. In addition, the optimal controller accelerates of the engine under high load which decreases fuel economy.

In the other hill tests, the total fuel consumptions of the controllers are almost the same, because both controllers reduce $\varepsilon_{m,\mathrm{com}}$ to 0.5. With the optimal controller, less fuel is consumed in steady-state driving, but this amount is lost when entering the hill as described above. Eventually, these are quite expected results, because the optimal controller is based on steady-state equations of the system.

6. Conclusions and future work

In this paper, we presented a fuel optimal controller for HSD based on the steady-state equations of the system, while including parts that consider dynamic situations as well. The devised controller was implemented in a 5-ton wheel loader to verify its efficacy and functionality. The fuel consumption of the machine was measured online with a state-of-the-art device.

The results of the optimal controller were compared to the ones obtained with a much simpler rule-based controller that is very similar to algorithms used in commercial wheel loaders. In steady-state driving, the optimal controller improved fuel economy at least 22.7% and up to 46.9%. Autonomous drive tests, including hills, different surfaces and loads, were also conducted, and the consumption was decreased up to 16.6%. Functionality of the controllers was proven in extreme hill climbing tests.

Even though the performance of the optimal controller was satisfactory at the conducted tests, it did not provide optimal behaviour in all situations. Especially, operation under rapidly increasing load was inefficient. However, further improvements require utilizing the dynamic equations of the system in the controller. Moreover, one important challenge is that the efficiency

curves of hydraulic components and BSFC curves of engines are only tested and provided in steady-state situations. It is known, as we also showed, that in dynamic situations actual consumption differs from steady-state curves. In the future, we will investigate MPC and consider dynamic equations of the HSD systems together with state and input constraint. This should provide better overall fuel economy, adequate velocity tracking, and no need for auxiliary functions at the output. In addition, we will also conduct complete work cycle experiments instead of pure driving in empirical tests.

Disclosure statement

No potential conflict of interest was reported by the authors.

Notes on contributors

Joni Backas graduated (MSc) from Tampere University of Technology in 2010, majoring in machine automation. Currently, he is a PhD student at the Department of Intelligent Hydraulics and Automation (IHA). His research interests lie in the control of hydrostatic drive transmissions, especially improving their fuel economy.

Reza Ghabcheloo received his PhD degree from Technical University of Lisbon, Portugal in 2007. He is currently an associate professor with the Department of Intelligent Hydraulics and Automation, Tampere University of Technology, Finland. His research interests include guidance and motion control for mobile robots, and optimal motion planning and control in particular for energy efficiency of hydraulic powertrains.

Seppo Tikkanen Seppo Tikkanen (MSc. 1995, Mech.Eng, Dr.Tech. 2000) is a professor of machine automation (energy efficient drives) in Department of Hydraulics and Automation at Tampere University of Technology. Previously he has worked as CTO at FIMECC Ltd., as group manager at Bosch Rexroth AG and as a researcher in Tampere University of Technology.

Kalevi Huhtala was born in August 1957. Received his Dr.Tech. degree from Tampere University of Technology (Finland) in 1996. He is currently working as a professor in the Department of Intelligent Hydraulics and Automation (IHA) at Tampere University of Technology. He is also the head of the department. His primary research fields are intelligent mobile machines and diesel engine hydraulics.

ORCID

Joni Backas http://orcid.org/0000-0002-0553-5990
Reza Ghabcheloo http://orcid.org/0000-0002-6043-4236
Seppo Tikkanen http://orcid.org/0000-0003-2973-094X
Kalevi Huhtala http://orcid.org/0000-0003-4055-0392

References

Ahopelto, M., *et al.*, 2013. Improved energy efficiency and controllability of mobile work machines by reduced engine rotational speed. *Proceedings of the ASME 2013 international mechanical engineering congress & exposition, IMECE2013*, San Diego, California, USA.

Ahopelto, M., Backas, J., and Huhtala, K., 2012. Power management in a mobile work machine: reduced diesel rpm for better energy efficiency. *Proceedings of the 7th FPNI PhD Symposium on Fluid Power*, June 27–30 2012, Reggio Emilia, Italy.

Arcadis, 2010. *Study in view of the revision of directive 97/68/EC on non-road mobile machinery (NRMM) (module I - an emissions inventory)*.

AVL, 2009. *AVL product description KMA mobile* [online]. Available from: https://www.avl.com/c/document_library/get_file?uuid=168caf92-827a-44ab-9dd2-33281cb4eb3dandgroupId=10138anddownload [Accessed 4 February 2015].

Backas, J., *et al.*, 2011. IHA-machine: a future mobile machine. *The proceedings of the twelfth scandinavian international conference on fluid power*. Tampere, Finland.

Backas, J., Ghabcheloo, R., and Huhtala, K., 10–12 September 2014. Fuel optimal controller for hydrostatic drives - a simulation study and model validation. *Proceedings of the Bath/ASME 2014 symposium on fluid power & motion control*, Bath, United Kingdom.

Bosch Rexroth AG, 2003. *Easy machine operation with rexroth automotive drive and anti stall control*. Elchingen: Bosch Group.

Catepillar Inc., 2013. *336E H hydraulic excavator* [online]. Available from: http://s7d2.scene7com/is/content/Caterpillar/C811713 [Accessed 20 April 2016].

Daher, N. and Ivantysynova, M., 2014. Energy analysis of an original steering technology that saves fuel and boosts efficiency. *Energy conversion and management*, 86, 1059–1068.

Deppen, T.O., Alleyne, A.G., Stelson, K.A. and Meyer, J.J., 2012. Optimal energy use in a light weight hydraulic hybrid passenger vehicle. *Journal of dynamic systems, measurement, and control*, 134 (4), 041009-1–041009-11. doi:http://dx.doi.org/10.1115/1.4006082.

Deppen, T.O., *et al.*, 2015. Comparative study of energy management strategies for hydraulic hybrids. *Journal of dynamic systems, measurement, and control*, 137 (4), 041002-1–041002-11. doi:http://dx.doi.org/10.1115/1.4028525.

Eaton Corporation, 2007. *ETAC: electronic transmission automotive control user's manual*. Eden Prairie, MN: Eaton Corporation.

Feng, D., Huang, D. and Li, D., 2011. Stochastic model predictive energy management for series hydraulic hybrid vehicle. *Proceedings of the 2011 IEEE international conference on mechatronics and automation*, Beijing, China.

Filipi, Z., *et al.*, 2004. Combined optimisation of design and power management of the hydraulic hybrid propulsion system for the 6 × 6 medium truck. *International journal of heavy vehicle systems*, 11 (3/4), 372–402.

Ghabcheloo, R., *et al.*, 2009. Autonomous motion control of a wheel loader. *ASME dynamic systems and control conference*, Hollywood, CA, USA.

Hippalgaonkar, R. and Ivantysynova, M., 2012. Fuel savings of a mini-excavator through a hydraulic hybrid displacement controlled system. *8th international fluid power conference, 8. IFK*, Dresden, Germany.

Huova, M., *et al.*, 2010. Energy efficient control of multiactuator digital hydraulic mobile machine. *7th international fluid power conference, 7. IFK*, Aachen, Germany.

Jalil, N., Kheir, N., and Salman, M., 1997. A rule-based energy management strategy for a series hybrid vehicle. *Proceedings of the American control conference*, Albuquerque, New Mexico.

Jähne, H., *et al.*, 2008. Drive line simulation for increased energy-efficiency of off-highway-machines. *6th international fluid power conference, 6. IFK*, Dresden, Germany.

KCMA Corporation, 2011. *Kawasaki loaders, CONEXPO 2011 handout* [online]. Available from: https://www.google.fi/url?sa=tandrct=jandq=andesrc=sandsource=webandcd=7andved=0CDYQFjAGahUKEwiAwZSgi7XHAhUF_HIKHdlrAGYandurl=http%3A%2F%2Fkawasakiloaders.com%2FdownloadFile.aspx%3Ffile%3D%2Fpublic%2FConExpo2011%2Fpdf%2FKawasaki_CONEXPO_Handout.pdfandei=j27UVcC9HoX4ywPZ1 [Accessed 19 August 2015].

Kermani, S., *et al.*, 2011. Predictive energy management for hybrid vehicle. *Control engineering practice*, 20 (4), 408–420.

Korane, K., 2004. *Machine design* [online]. Available from: http://machinedesign.com/archive/getting-more-mobile-machines [Accessed 21 December 2015].

Kum, D., Peng, H., and Bucknor, N.K., 2011. Supervisory control of parallel hybrid electric vehicles for fuel and emission reduction. *Journal of dynamic systems, measurement, and control*, 133 (6), 061010-1–061010-10. doi: http://dx.doi.org/10.1115/1.4002708.

Kumar, R. and Ivantysynova, M., 2011. An instantaneous optimization based power management strategy to reduce fuel consumption in hydraulic hybrids. *International journal of fluid power*, 12 (2), 15–25.

Luomaranta, M., 1999. A stable electrohydraulic load sensing system based on a microcontroller. *The proceedings of the sixth Scandinavian international conference on fluid power*, 26–28 May 1999, Tampere, 419–432.

Meyer, J., *et al.*, 2010. Power management strategy for a parallel hydraulic hybrid passenger vehicle using stochastic dynamic programming. *Proceedings of the 7th international fluid power conference*, Aachen, Germany.

Opila, D., *et al.*, 2013. Real-time implementation and hardware testing of a hybrid vehicle energy management controller based on stochastic dynamic programming. *Journal of dynamic systems, measurement, and control*, 135 (2), 021002-1–021002-11. doi:http://dx.doi.org/10.1115/1.4007238.

Paganelli, G., *et al.*, 2001. General supervisory control policy for the energy optimization of charge-sustaining hybrid electric vehicles. *JSAE review*, 22 (4), 511–518.

Paganelli, G., *et al.*, 2000. Simulation and assessment of power control strategies for a parallel hybrid car. *Proceedings of the institution of mechanical engineers, part D: journal of automobile engineering*, 214 (7), 705–717.

Pfiffner, R., Guzzella, L., and Onder, C., 2003. Fuel-optimal control of CVT powertrains. *Control engineering practice*, 11 (3), 329–336.

Sciarretta, A., Back, M., and Guzzella, L., 2004. Optimal control of parallel hybrid electric vehicles. *IEEE transactions on control systems technology*, 12 (3), 352–363.

Sciarretta, A. and Guzzella, L., 2007. Control of hybrid electric vehicles. *IEEE control systems magazine*, 27 (2), 60–70.

Serrao, L., Onori, S., and Rizzoni, G., 2011. A comparative analysis of energy management strategies for hybrid electric vehicles. *Journal of dynamic systems, measurement, and control*, 133 (3), 031012-1–031012-11. doi:http://dx.doi.org/10.1115/1.4003267.

Srivastava, N. and Haque, I., 2009. A review on belt and chain continuously variable transmissions (CVT): dynamics and control. *Mechanism and machine theory*, 44 (1), 19–41.

The Lubrizol Corporation, 2013. *John Deere adopts hybrid technology* [online]. Available from: http://drivelinenews.com/off-highway-insights/john-deere-adopts-hybrid-technology/ [Accessed 19 August 2015].

Wang, Y., Zhang, H., and Sun, Z., 2013. Optimal control of the transient emissions and the fuel efficiency of a diesel hybrid electric vehicle. *Proceedings of the institution of mechanical engineers part D: journal of automobile engineering*, 227 (11), 1547–1561.

Williamson, C. A., 2010. *Power management for multi-actuator mobile machines with displacement controlled hydraulic actuators*. Thesis (PhD). Purdue University.